Food Chemistry 455 (2024) 139769

Contents lists available at ScienceDirect

Food Chemistry

journal homepage: www.elsevier.com/locate/foodchem

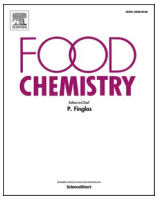

Unraveling the antifungal composition of bitter orange decoction against the melon pathogen *Fusarium jinanense*

Maria Daiane de Freitas [a,1], Rodolfo Dantas Lima Junior [b,1], Francisco Erivaldo Freitas da Silva [a], Eliane Mayumi Inokuti [c], Andréia Hansen Oster [d], Davila Zampieri [a], Cristiano Souza Lima [c], Taicia Pacheco Fill [b], Telma Leda Gomes de Lemos [a,*]

[a] Departamento de Química Orgânica e Inorgânica, Universidade Federal do Ceará, Campus do Pici, 60021-940, Fortaleza, Ceará, Brazil
[b] Instituto de Química, Universidade de Campinas, 13083-970, Campinas, SP, Brazil
[c] Departamento de Fitotecnia, Universidade Federal do Ceará, Campus do Pici, 60440-554, Fortaleza, Ceará, Brazil
[d] Empresa Brasileira de Pesquisa Agropecuária, Embrapa Uva e Vinho, 95701-008, Bento Gonçalves, Rio Grande do Sul, Brazil

ARTICLE INFO

Keywords:
Citrus aurantium
Phenolic compounds
Molecular networking
SIRIUS
Anti-phytopathogenic activity
Fusarium rot melon

ABSTRACT

Bitter orange (*Citrus aurantium*) is an important source of essential oils with high antimicrobial activities, however the composition and antifungal potential of the decoction peels is little explored. This study assessed the peel decoction's chemical profile at the secondary metabolism level and its antifungal activity against the melon phytopathogen *Fusarium jinanense*. The decoction's antifungal potential was investigated using a bioassay-guided fractionation approach based on Solid-Phase Extraction (SPE) and LC-HRMS/MS analysis. Coumarins and flavones were the most abundant classes of compounds in the high-value fractions responsible for up to 61% of the mycelial inhibition of *F. jinanense*. Overall, this study has presented for the first time the chemical composition, the antifungal potential of the decoction of *C. aurantium* peels and the compounds associated with these results. This strategy can guide the exploration of under-explored food sources and add value to compounds or fractions enriched with bioactive compounds.

1. Introduction

The citrus industry is essential to Brazil's fruit industry, with 137.5 million tonnes of citrus exported in 2019, including lemons, limes, oranges, pomelos, and tangerines (FAO-Food and Agriculture Organization, 2020). In 2021, Brazil exported 3.5 thousand t of fresh oranges and 22.5 million t of orange juice, produced mainly by São Paulo, Minas Gerais, and Paraná states. These numbers figures position the country as the world's leading producer of fresh oranges and the world's largest exporter of orange juice, ahead of countries such as the United States and China (Kist, Carvalho, & Beling, 2022).

Among the varieties of orange species, *Citrus aurantium* L., typically known as bitter orange or sour orange, is a Southeast Asia native species that belongs to the Geraniales order and the Rutaceae family (Degirmenci & Erkurt, 2020). Although the fruit has a bitter pulp and is not commonly used for juices, it has a variety of applications, including obtaining essential oils, and food supplements (Deterre, Rega, Delarue, Teillet, & Giampaoli, 2014; Onakpoya, Davies, & Ernst, 2011; Oulebsir, Mefti-Korteby, Djazouli, Zebib, & Merah, 2022).

Literature reports the antimicrobial action of *C. aurantium* essential oil against different microorganisms, including phytopathogenic fungi of important crops, such as *Aspergillus flavus*, *Aspergillus niger*, *Aspergillus terreus*, and *Fusarium culmorum* (Abo Elgat et al., 2020). In addition, Perczak et al. (2019) and Okwu, Awurum, & Okoronkwo, 2007 verified the antifungal potential of *C. aurantium* essential oil against strains of the *Fusarium* genus (*Fusarium graminearum*, *Fusarium culmorum,* and *Fusarium oxysporum*).

Fungi of the *Fusarium* genus are associated with plant diseases of various tropical fruit crops such as avocado, banana, mango, pineapple, and yellow melon (Zakaria, 2023). The yellow melon (*Cucumis melo*) is one of the most economically important crops worldwide. According to the FAO, in 2021, Brazil produced 607,000 t of melons and exported 257,000 t of fruit, which corresponded to 165,000 dollars. The primary melon production in Brazil is concentrated in the Northeast region,

* Corresponding author.
E-mail address: tlemos@dqoi.ufc.br (T.L. Gomes de Lemos).
[1] The authors equally contributed.

https://doi.org/10.1016/j.foodchem.2024.139769
Received 12 March 2024; Received in revised form 4 May 2024; Accepted 19 May 2024
Available online 24 May 2024

which accounts for around 95% of the Brazilian production, with the State of Rio Grande do Norte as the leading producer (Kist et al., 2022; IBGE-Brazilian Institute of Geography and Statistics, 2023; Medeiros Araújo et al., 2021). However, in Brazil, pathogens of the *Fusarium* genus are responsible for significant losses in melon production. New fungal species from the *Fusarium incarnatum-equiseti* species complex (FIESC) have now been discovered, such as *Fusarium jinanense* Han, Wang & Cai, capable of causing fruit rot that can compromise production in the post-harvest stage (Han et al., 2023; Lima et al., 2021).

Despite the variety of applications of *C. aurantium* as a source of bioactive compounds against fungi of the *Fusarium* genus, to date, no studies have been focused on the chemical composition and the antifungal potential of the decoction obtained from the peel of the fruit against phytopathogens of this genus. Thus, here we integrated a bio-guided fractionation strategy based on solid-phase extraction with high-performance platforms such as liquid chromatography coupled with mass spectrometry and analysis by Feature-Based Molecular Networking (FBMN) to add value to this little-exploited by-product and, above all, to identify, using a Global Natural Product Social Molecular Networking (GNPS) repository and SIRIUS software, which compounds are involved in the antifungal potential against *Fusarium jinanense*, the causal agent of yellow melon rot.

2. Materials and methods

2.1. Reagents and materials

Ethyl acetate (EtOAc) and methanol (MeOH) were purchased from Synth (Diadema, Brazil), while acetone (HPLC-grade) was obtained from Tedia Company (Fairfield, USA). HPLC-MS-grades solvents (methanol and acetonitrile (ACN)) and formic acid were used while ultrapure water (18 MΩ cm at 23 °C) was prepared using a Milli-Q purification system (Merck Millipore; Burlington, MA, USA). Potato dextrose agar (PDA) was purchased from KASVI™ (São José do Pinhais, Brazil). Antifungal Cercobin® 875 WG was purchased from Iharabras S.A. (Indústrias Químicas, Sorocaba, Brazil). PTFE (0.22 μm) membrane syringe filters (Millipore) were bought from Merck Millipore Co., Ltd. (Cork, Ireland). The chromatography column (C18) was obtained from Bruker Daltonics (Bruker, Bremen, Germany). The standards naringin, hesperidin, and hesperitin were purchased from Sigma Aldrich (St. Louis, MO, USA).

2.2. Citrus sample and preparation of the crude extract

Specimens of *C. aurantium* fruits were collected at the Department of Plant Sciences of the Federal University of Ceará (UFC), with the following coordinates (3.7406° S, 38.5764° W), Campus do Pici in Fortaleza, Ceará, Brazil on the 26th September 2019 at 3:45 pm. The exsiccates are deposited in the Prisco Bezerra Herbarium under number 50434.

Twelve oranges were collected and properly rinsed with deionized water. The orange peels were separated into flavedo and albedo fractions using a vegetable peeler. This resulted in 398 g of flavedo, which was decocted with 3 L of distilled water and refluxed for 3 h. Subsequently, a simple filtration was carried out, and the decoction obtained was partitioned with ethyl acetate, where for every 100 mL of the aqueous fraction, 100 mL of solvent was used three times. The partitions were concentrated under reduced pressure in a rotary evaporator with a bath temperature of 40 °C.

2.3. Fractionation-based SPE

The crude decoction extract (CDE) was fractionated through the solid phase extraction process using a cartridge (Strata™ C18, 20 g/60 mL, 55 μm, 70 Å) supplied by Phenomenex (Torrance, CA, U.S.A). The cartridge was previously activated using 10 mL of MeOH and adjusted with 10 mL of H_2O/MeOH (80:20, v/v) as already described in the literature (Nair & Clarke, 2016). Then, 100 mg of the extract was subjected to chromatography, using 150 mL of eluent per fraction H_2O/MeOH (80:20; 50:50; 20:80; 0:100) and CH_3COCH_3 (100), resulting in five fractions that they were named FR1, FR2, FR3, FR4, and FR5, respectively. The CDE and fractions samples were subjected to antifungal assay against the phytopathogen *F. jinanense* (UFCM-0611).

2.4. Fungal isolate

The isolate UFCM-0611 of *F. jinanense* (isolate 41 or LPPC072 in Lima et al., 2021) was obtained in the 2015's growing season from yellow melon fruit showing typical symptoms of fusarium rot in Maracanaú city in Ceará State, Brazil. Species identification and pathogenicity assay were carried out according to the methodology described by Lima et al. (2021) and Han et al. (2023). The isolate (UFCM-0611) is maintained at the Federal University of Ceará Mycological Collection (UFCM), Department of Plant Sciences, Fortaleza, Ceará, Brazil.

2.5. Antifungal assays of the extract and fractions

The *in vitro* antifungal assay of the CDE and fractions FR1-FR5 against *F. jinanense* (UFCM-0611) was performed using a potato dextrose agar (PDA) culture medium. The PDA was sterilized in an autoclave at 101 KPa (120 °C) for 15 min. Subsequently, the extract and fractions were solubilized separately in methanol (100 μL) and added to molten (45 °C) PDA medium at three concentrations: 50, 100, and 150 ppm. The commercial fungicide Cercobin (active ingredient: methyl thiophanate) was used as a positive control. For this, the fungicide was dissolved in sterilized distilled water. Then, serial dilutions were performed to obtain thiophanate methyl solutions at three concentrations (50, 100, and 150 ppm). Mycelial plugs (3 mm in diameter) were removed from the margins of a four-day-old culture of UFCM-0611 and transferred to the center of the wells in the plates amended with the different concentrations of the crude extract, fractions and fungicide used as positive control. Wells on the plates containing only PDA and mycelial plugs (3 mm in diameter) were used as a negative control.

All treatments were performed using technical replicates in triplicate. Tests were also conducted using only methanol as negative control. After a 25 h incubation period at 25 °C and under a 12 h photoperiod, the diameter of the colonies was measured, and the mean of two perpendicular mycelial-growth diameters for each replicate was calculated. The original diameter of the mycelial plug (3 mm) was subtracted from this measurement. The percentage of inhibition of radial mycelial growth (% IR) related to the negative control was calculated for all the tested concentrations. The rate of radial growth (IR) was determined according to Simionato et al. (2017) using the formula below.

$$\%IR = \frac{Dc - Dt}{Dc}\ x\ 100$$

where Dc = average diameter of the fungal mycelial of the negative control (methanol), Dt = average diameter of the fungal mycelial treated with the extracts or the positive control. Only the fractions that showed promising results in the antifungal tests and the CDE were analyzed by LC-MS/MS.

2.6. UHPLC-MS/MS analysis and data processing

Samples of the CDE and fractions FR3 and FR4 were weighed (1.0 mg), solubilized in 1.0 mL of MeOH (HPLC grade), and filtered through a PTFE 0.22 μm filter. UHPLC-MS/MS data were obtained using a Thermo Fisher RSLCnano U3000 UHPLC instrument coupled with a Q-Exactive Orbitrap-MS spectrometer (Thermo Fisher Scientific, Waltham, MA, USA) equipped with a heated electrospray ionization (HESI) source. The chromatographic elution was performed using a Intensity Solo C18 column (Bruker Daltonics, Bremen, Germany) with the following specifications: 100 mm × 2.1 mm, 2.2 mm particle size. The mobile phase

flow was maintained at 250 μL/min at 40 °C. A mixture of H_2O (A) and MeCN (B), both acidified with 0.1% formic acid, was used as a mobile phase. The elution gradient for the positive and negative modes consisted of 5% B (0–5 min), 5–40% B (5–10 min), 40–45% B (10–12 min), 45–98% B (12–18 min), 98% B (18–20 min), 98–5% B (20–22 min) and 5% B (22–24 min).

The samples were analyzed in Full-scan mode and DDA (data-dependent acquisition) mode with a range of *m/z* 100–1500 Da. Ionization was carried out in positive and negative ionization modes, with the following parameters: auxiliary gas flow, 10 (arbitrary unit); spray voltage +3.5 kV (positive mode) and − 3.2 kV (negative mode); capillary temperature of 300 °C, equipment resolution of 70,000 (200 *m/z*). MS/MS data were acquired by selecting five precursors per cycle and normalized collision energy (NCE) of 30 eV. The Q-Exactive Orbitrap-MS was operated using the Xcalibur 3.0 software (Thermo Fisher Scientific, Waltham, MA, USA).

Next to the positive mode ionization analysis, the raw data files (.raw) were converted to .mzXML format using MSConvert (ProteoWizard, Palo Alto, CA, USA) (Adusumilli & Mallick, 2017). After that, the files (.mzXML) were submitted for processing by MZmine (version 2.53) (Pluskal, Castillo, Villar-Briones, & Oresic, 2010) using feature detection, chromatogram builder, chromatogram deconvolution, isotope grouping, alignment, and filtering. The values for these parameters can be consulted in the supplementary material (**Supplementary Table 1**). After processing, files containing a quantification table of the detected features (.csv) were exported, as well as a file (.mgf) containing the MS/MS data information associated with the precursor ions (MS). The files were submitted for analysis on the Global Natural Products Social Molecular Networking (GNPS) platform (https://gnps.ucsd.edu) to annotate the features belonging to the samples and obtain molecular networks based on the similarity of the fragmentation profile of the features.

2.7. Feature-based molecular networking analysis and metabolite annotation

To evaluate the chemical composition of the crude extract and fraction samples, the processed UHPLC-MS/MS data (.csv and .mgf) from MZmine 2.53, together with a metadata table containing the main characteristics of the samples (.tsv), were processed for molecular networking creation based on Feature-Based Molecular Networking (FBMN) workflow on the GNPS platform (Nothias et al., 2020). The parameters are present in (**Supplementary Table 2**). The FBMN job on GNPS can be found at https://gnps.ucsd.edu/ProteoSAFe/status.jsp?task=f336f310b7314351bdacdfc7a2288a11.

The molecular network obtained was visualized using the Cytoscape software (version 3.7.2, Cytoscape Consortium, San Diego, CA, United States) (Shannon et al., 2003), where each node corresponds to ion features of specific *m/z* ratio and retention time. The edges represent the similarity cosine scores calculated between the nodes based on the fragmentation spectra (MS/MS). The node size was scaled proportionally to the relative sum of the peak areas obtained in the samples where the feature was detected. The edge width was adjusted proportionally to the cosine of the similarity between the nodes, which ranged from 0.7 to 1.0. The nodes were represented in the network as a pie chart, where the colors were associated with sample groups: crude decoction extract (CDE), fraction 3 (FR3), and fraction (FR4).

The annotation of the compounds was performed according to the annotation levels reported by Metabolomics Standards Initiative (MSI) (Fiehn et al., 2007; Sumner et al., 2007), using the GNPS library and a manual curation from the comparison of the mass accuracy with a mass tolerance of 5 ppm for MS1 and characteristic fragments (MS/MS). Manual dereplication was performed using reference spectral data of substances produced in *C. aurantium* species and already reported in the ACS publication, Google Scholar, SciELO, Science Direct, Springer, Web of Science, Massbank, and Pubchem. The data obtained were compared with precursor mass ions (MS1) and the mass fragments ions (MS/MS) contained in the CDE, FR3, and FR4 samples. The molecular formula of the ion fragments was predicted using the "elementary composition" provided by the Xcalibur 3.0 software (Thermo Fisher Scientific, Waltham, MA, USA), considering an error of ±5 ppm for positive and negative modes.

The SIRIUS software (version 4.0.1) (Dührkop et al., 2019) was used to explore possible chemical structures of substances corresponding to the obtained features and the prediction of molecular formulas associated with these features. The structure propagation of the compounds occurred from comparing the isotopic distribution of the precursor ions and *in silico* prediction of the molecular formulas and fragments acquired in the LC-MS/MS analysis with a library of experimental and *in silico* data. The molecular formula prediction by ZODIAC, molecular structure prediction based on CSI:FingerID, and, finally, chemical class evaluation by CANOPUS were used for this data set. The parameters used to predict the formula took into account the possible adducts associated with the feature ($[M + H]^+$, $[M + H\text{-}H_2O]^+$, $[M + Na]^+$, and $[M + K]^+$), the analyzer used (Orbitrap), the maximum error in ppm (5 ppm), and the association of features with molecular formulas present in databases (Bio database).

3. Results and discussion

3.1. SPE fractionation of Citrus aurantium peels decoction revealed a potent inhibition of Fusarium jinanense

After obtaining 1.4270 g of crude decoction extract (CDE) (yield 0.36%, w/w), 100 mg of the CDE was subjected to the SPE fractionation method where five fractions were obtained: FR1 (19.6 mg), FR2 (49.8 mg), FR3 (15.5 mg), FR4 (5.3 mg) and FR5 (3.2 mg). In order to select the fractions with the highest antifungal activity against *F. jinanense* (UFCM-0611), the mycelial inhibition potential of each fraction was compared with the positive control containing the active ingredient methyl thiophanate. Methyl thiophanate is currently used as a synthetic fungicide (Cercobin®) to control fungal diseases in yellow melon.

The antifungal microdilution plate assay showed potent inhibition of the mycelial growth of the pathogenic fungus for fractions 3 and 4 compared to the positive control in a concentration range of 100–150 ppm. Compared to the inhibition values obtained for the crude extract in the same concentration range tested, it was possible to observe an increased antifungal effect after fractionation. Tests performed at 100 ppm showed inhibition of 51% (FR3) and 46% (FR4) compared to 42% for crude extract under the same conditions. At a concentration of 150 ppm, the activity of fraction 3 (MeOH:H_2O fraction (80:20)) and fraction 4 (MeOH fraction) was higher than that of crude extract, reaching 61% (FR3) and 57% (FR4), respectively, in comparison with 50% for crude extract. Compared to the inhibition values obtained for the positive control at 100 ppm (35%) and 150 ppm (48%), fractions 3 and 4 showed higher results of 51% and 46% (100 ppm), and 61% and 57% (150 ppm), respectively. Fig. 1 illustrates the results presented and outlines the clear statistically significant difference in antifungal activity between the extract and the active fractions at different concentrations compared to the positive control under the same conditions. Graphs showing the inhibition percentage of all fractions tested are provided in the supplementary material **(Supplementary Fig. 1)**. Based on these results, samples of the crude extract and fractions 3 and 4 were then selected for analysis by UHPLC-MS/MS to verify the variation in chemical composition after fractionation and thus be able to associate the bioactivity observed with the active compounds present in each fraction.

3.2. Active fractions and crude extract chemical profiles

From the UHPLC-MS/MS analyses of the active fractions and the CDE, it was possible to observe the separation capacity, preconcentration, differentiation of the chemical profile, and composition

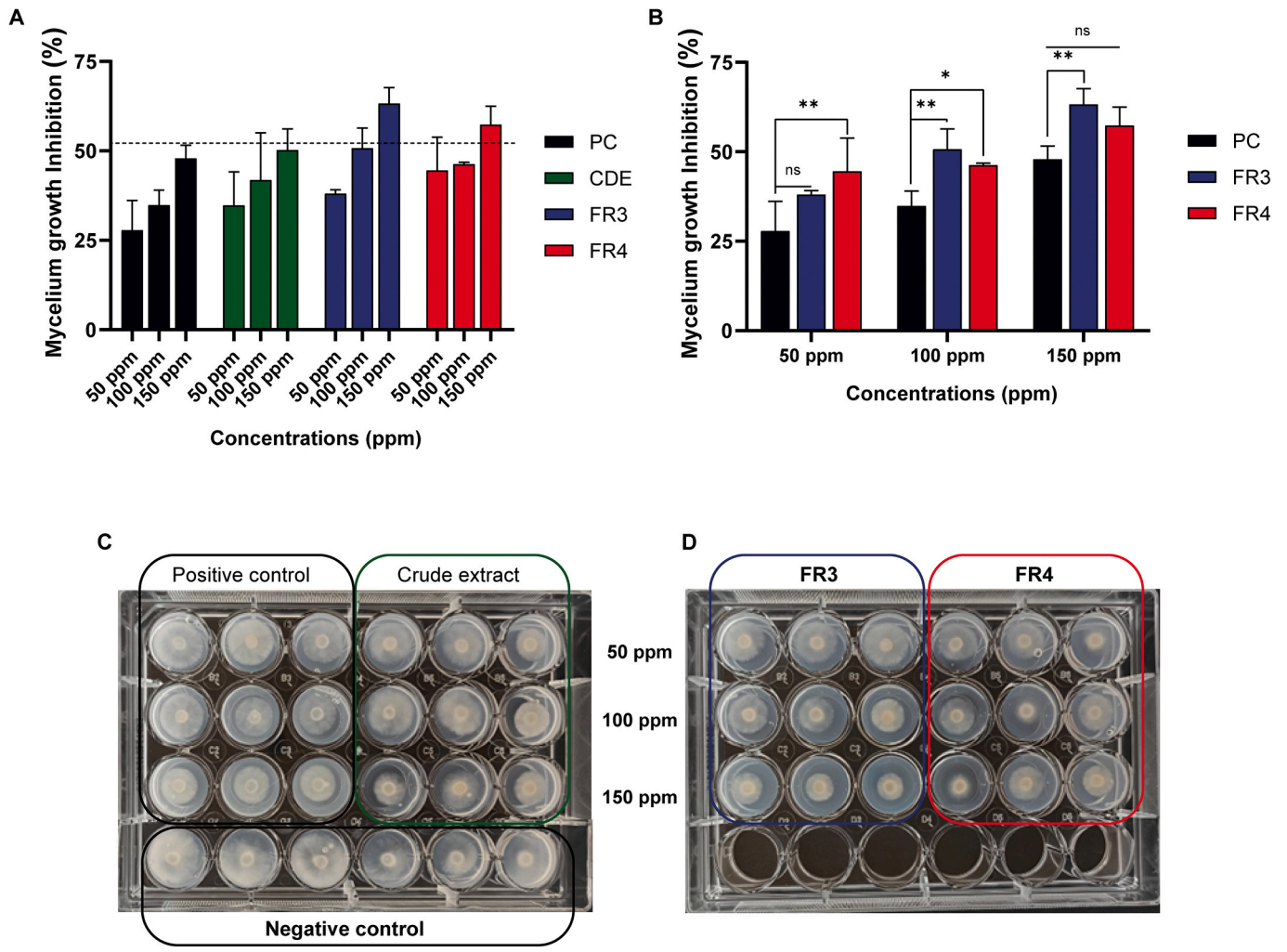

Fig. 1. Crude decoction extract (CDE) and fractions of *Citrus aurantium* peels showed potent dose-dependent inhibition of mycelial growth of *Fusarium jinanense*. **A.** Antifungal microdilution plate assay at concentrations of 50, 100, and 150 ppm for the CDE, fraction 3 (FR3), fraction 4 (FR4), and the positive control (PC) methyl thiophanate. The dashed black line emphasizes the level of mycelial growth inhibition for positive control. **B.** Inhibition potential of mycelial growth of *F. jinanense* using the most active fractions (FR3 and FR4) compared to the positive control at different concentrations (50, 100, and 150 ppm). Statistical analysis: ANOVA was performed with post-hoc Tukey's multiple comparisons tests. *, ** and ns = statistically significant differences with $p < 0.05$, $p < 0.005$, and no significant, respectively. **C** and **D.** Photos of the microdilution plate assay after 72 h.

of the samples after fractionation by SPE from 100 mg of the crude extract. The chromatograms in positive ionization mode presented in Fig. 2 show the success of the fractionation based on the evident differentiation of the relative abundances associated with the secondary metabolites present at different retention times.

This pattern is highlighted in the base peak chromatograms (BPC) of FR3, where it was possible to see a decrease in the abundance of the metabolites present in the 10–12 min range compared to the crude extract. For fraction 4, eluted with 100% methanol, there was a decrease in the relative abundance of the secondary metabolites between 13 and 14.5 min in FR3. The variation in relative abundances throughout the fractionation shows important physicochemical characteristics about the nature of the compounds involved in the antifungal activity observed for these fractions, such as intermediate polarity, which is directly related to the molecular structure of the secondary metabolites analyzed, and affinity with the long carbon chains contained in the stationary phase of the SPE cartridge (C18).

To summarize, the increase in antifungal activity against *F. jinanense* observed in fractions 3 and 4 is directly related to the contribution of the SPE fractionation, which reduces the complexity of the chemical composition of the starting samples and the consequent preconcentration of compounds with intermediate polarity, compared to the distribution of these compounds in the crude extract.

The molecular networks obtained from the FBMN workflow for the positive ionization mode were analyzed to better understand the composition of the crude extract and the active fractions and to point out which compounds may be involved in the antifungal activity based on the distribution of these metabolites after fractionation. The molecular network was generated with 605 precursor ions and their respective fragmentation spectra, responsible for forming 48 spectral families (clusters) and 348 self-loops nodes (**Supplementary Fig. 2**). Comparison of the MS/MS spectra of these nodes with the GNPS spectral library generated 50 spectral matches for the positive mode, corresponding to 8.26% of the total nodes that comprise the entire molecular network. All fragmentation spectra associated with a spectral match to the GNPS library were evaluated for annotation at confidence level 2 (Schymanski et al., 2014), and manual curation of the spectra was performed according to previous literature for this citrus cultivar. The GNPS library's annotations of features with secondary metabolite matches that still need to be reported for the species were considered level 3 annotations (Schymanski et al., 2014). The annotated metabolites are listed in Table 1, and their spectral matches are in the **Supplemental Material**.

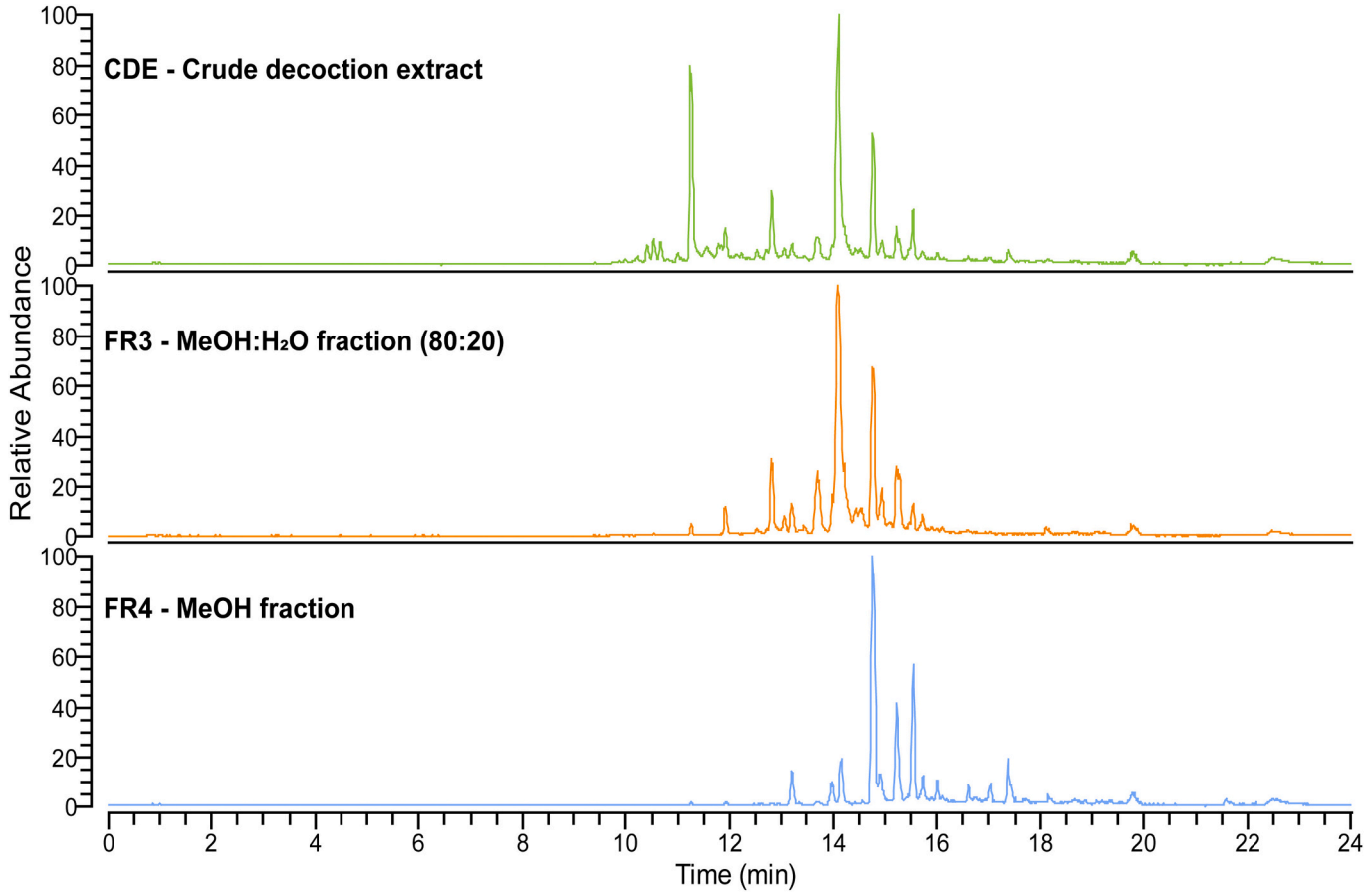

Fig. 2. Chemical profile through base peak chromatograms (BPCs) obtained from crude decoction extract (CDE) and active fractions (FR3 and FR4) from *Citrus aurantium* L. in positive ionization mode. BPCs from the ethyl acetate CDE are shown on the top (green), and those of the active fractions 3 and 4 obtained from proportions MeOH:H_2O (80:20) and MeOH (100%) are shown in orange and blue, respectively. (For interpretation of the references to colour in this figure legend, the reader is referred to the web version of this article.)

3.3. Putative annotation and identification of compounds by UHPLC-MS/MS from Citrus aurantium peels with potential antifungal activity

LC-MS/MS analysis of the ethyl acetate extract of the decoction and active fractions allowed the annotation of 57 compounds in the positive ionization mode and eight in the negative mode with confidence levels 1, 2, and 3 (**Supplementary Table 3**). The annotation matches of the compounds from the GNPS library indicated the presence of different classes of substances including flavonoids, limonoids, coumarins, terpenes, aromatic compounds, and nitrogen-containing compounds. Among the annotated compounds, 36 are flavonoids belonging to the flavone, flavanone, and flavonol subclasses; 17 were classified as coumarins, and the remaining 12 compounds are distributed among other classes, as shown in Table 1 and **Supplementary Table 3**. In addition to the annotation based on the similarity of fragmentation patterns obtained by tandem mass spectrometry (MS/MS) analysis using the GNPS library, the chemical structures of 23 compounds from the flavonoid (12) and coumarin (11) classes were proposed from the annotation propagation based on GNPS annotations, the construction of the molecular network and the construction of fragmentation trees using the CSI:Finger ID module of the SIRIUS software (**Supplementary Table 4 and 5**). This tool uses a pipeline based on constructing fragmentation trees from MS/MS spectra of a training dataset to construct fingerprints (molecular properties), as well as constructing fragmentation trees and fingerprints from the experimental dataset. Finally, the similarity of the fingerprints of the compounds to be identified (experimental) is searched against fingerprints from databases such as PubChem, with the aim of predicting different structures with a high similarity index through the confidence score (Dührkop et al., 2019). All the structural proposals provided by the SIRIUS software were based only on nodes present in molecular networks containing level 2 annotations obtained from the GNPS spectral library. This strategy allowed to gain insights concerning the chemical composition of the active fractions based on the fragmentation trees proposed for each compound.

3.3.1. Flavones, flavanones, and flavonols

Several molecular families and self-loops related to the flavonoid class were obtained, including flavonoids *O*-glycosylated of the flavanones, flavones, and flavonols subclasses, which can be observed by the several green coloring nodes in the molecular network (Fig. 3).

From the analysis of the molecular network and manual curation, it was possible to observe the presence of a greater abundance of *O*-glycosylated flavonoids (compounds 3, 6, 8, 10, 11, 12, 13, 16, 17, 19, 21 and 22 (Table 1)), and compounds 3N, 4N, 5N and 6N (**Supplementary Table 3**) in nodes corresponding to the CDE sample, indicating that after fractionation by SPE these compounds remained in the initial fractions containing more aqueous character (FR1 and FR2) than when compared to the final fractions with more organic character (FR3 and FR4).

Glycosylated flavonoids are highly polar compounds containing mono- or disaccharides modified or not by other substituents, which do not favor interaction with the C-18 stationary phase used in SPE, thus facilitating rapid elution with a predominantly aqueous mobile phase gradient.

The typical fragmentation of these protonated molecules involves the sugar moiety loss, as shown in the tandem mass spectra (MS/MS) (**Supplementary Fig. 6, 9, 13, 17, 19, 21, 22, 25, 28, 29, 31, 33, 34,**

Table 1
Annotation of secondary metabolites in the *Citrus aurantium* L. peel decoction extract and its fractions by manual dereplication and based on spectral matches within the GNPS platform.

Feature	R_t (min)	$[M+H]^+$; $^2[M+H\text{-}H_2O]^+$; $^3[M+NH_4]^+$; $^4[M+Na]^+$								
		Theoretical mass (*m/z*)	Measured mass (*m/z*)	MS/MS	Error (ppm)	Molecular formula[a]	Annotation	FR3	FR4	Node	Ref.
1	9,96	211.1446	211.1442	183, 138, 114, 98, 86	−1.894	$C_{11}H_{18}O_2N_2$	❖Dipeptide[c]	–	–	8230	CCMSLIB00005739084
2	9.97	289.0707	289.0708	289, 153, 145	0.346	$C_{15}H_{12}O_6$	Eriodictyol[b]	–	–	–	Yu et al., 2020
3	10.0	597.1819	597.1818	289, 195, 153, 399	−0.167	$C_{27}H_{32}O_{15}$	Eriocitrin[c]	–	–	8029	CCMSLIB00010124324
4	10.09	183.0657	183.0655	155, 140, 123, 95	−1.093	$C_9H_{10}O_4$	Syringaldehyde[c]	–	–	8269	CCMSLIB00003136460
5	10.21	193.0500	193.0498	178, 165, 149, 137, 133	−1.036	$C_{10}H_8O_4$	Isoscopoletin [c]	–	–	8072	CCMSLIB00006417685
6	10.27	581.1865	581.1869	435, 383, 273, 153, 121	0.688	$C_{27}H_{32}O_{14}$	Naringin[b]	x	x	–	Wang et al., 2021
7	10.35	193.0500	193.0498	178, 165, 161, 149, 133	−1.036	$C_{10}H_8O_4$	Scopoletin[c]	–	–	8153	CCMSLIB00005778023
8	10.35	579.1708	579.1713	433, 271, 153	0.863	$C_{27}H_{30}O_{14}$	Rhoifolin[b]	–	–	–	Kim et al., 2023
9	10.39	273.0757	273.0759	273, 147, 153, 119	0.732	$C_{15}H_{12}O_5$	Naringenin[b]	x	x	–	Kim et al., 2023
10	10.41	595.1657	595.1654	431, 287, 263, 161, 153	−0.504	$C_{27}H_{30}O_{15}$	Luteolin 7-*O*-neohesperidoside[b]	–	–	–	Mencherini et al., 2013
11	10.41	435.1286	435.1288	273, 153, 145	0.460	$C_{21}H_{22}O_{10}$	Naringenin-*O*-glucoside[d]	x	–	6534	CCMSLIB00010113073
12	10.42	598.2135[3]	598.2133[3]	273, 171, 153, 147, 85	−0.334	$C_{27}H_{32}O_{14}$	❖Flavanone[c]	x	–	6905	CCMSLIB00000845824
13	10.46	479.1189	479.1187	317, 302, 285, 145, 127	−0.417	$C_{22}H_{22}O_{12}$	❖Flavonol[cs]	–	–	8479	CCMSLIB00004718647
14	10.55	175.0371[4]	175.0393[4]	147, 119, 91	5.666	$C_8H_8O_3$	Vanillin[c]	–	–	8516	CCMSLIB00006357163
15	10.55	409.1498	409.1496	247, 229, 187, 175	−0.488	$C_{20}H_{24}O_9$	❖Furocoumarin[c]	x	x	3959	CCMSLIB00000846145
16	10.62	611.1970	611.1971	303, 195, 153, 85	0.163	$C_{28}H_{34}O_{15}$	Hesperidin	x	x	–	Yu et al., 2020
17	10.64	449.1442	449.1443	303, 153,129	0.223	$C_{22}H_{24}O_{10}$	Hesperetin-*O*-rhamnoside[b]	x	–	–	Yu et al., 2020
18	10.71	463.1235	463.1238	445, 427, 397, 367, 343	0.648	$C_{22}H_{22}O_{11}$	Diosmetin-8-*C*-glucoside[b]	x	–	5444	Wen et al., 2021
19	10.86	753.2242	753.2240	301, 145, 127, 103, 85	-0.265	$C_{34}H_{40}O_{19}$	❖Flavonol[c]	–	–	8368	CCMSLIB00004718799
20	10.95	531.1502	531.1502	177, 163, 149, 145, 135	0.000	$C_{26}H_{26}O_{12}$	❖Cinnamic acids derivatives[cs]	–	–	8796	CCMSLIB00000848797
21	10.99	772.2664[3]	772.2660[3]	345, 303, 171, 127, 85	−0.518	$C_{34}H_{42}O_{19}$	❖Flavanone[c]	–	–	8621	CCMSLIB00000848270
22	11.18	479.1189	479.1186	317, 302, 153	−0.626	$C_{22}H_{22}O_{12}$	❖Flavonol[cs]	–	–	8355	CCMSLIB00000221170
23	11.24	243.1021[2]	243.1016[2]	201, 189, 173, 159, 131	−2.057	$C_{15}H_{16}O_4$	Auraptenol[c] or CHEMBL3590439[sp], or Micromarin F[s]	–	–	8010	CCMSLIB00005722959
24	11.24	261.1126[2]	261.1125[2]	243, 217, 201, 189, 131	-0.383	$C_{15}H_{18}O_5$	Meranzin Hydrate or Ulopterol[ds]	–	–	8007	CCMSLIB00005722913
25	11.29	261.1126	261.1124	243, 189, 131, 103	-0.766	$C_{15}H_{16}O_4$	Meranzin[b]	x	x	–	Wang et al., 2021
26	11.54	257.0813	257.0810	171, 153, 131, 103, 67	-1.167	$C_{15}H_{12}O_4$	Pinocembrine[c]	x	–	6603	CCMSLIB00010116989
27	11.78	203.0339	203.0341	175, 147, 119	0.985	$C_{11}H_6O_4$	Xanthotoxol[b]	x	x	–	Yu et al., 2020
28	12.35	271.0601	271.0605	271, 153, 119, 91	1.476	$C_{15}H_{10}O_5$	Apigenin[b]	–	–	–	Horai et al., 2010

Feature	R_t (min)	$[M+H]^+$; $^2[M+H\text{-}H_2O]^+$; $^3[M+NH_4]^+$; $^4[M+Na]^+$									
		Theoretical mass (*m/z*)	Measured mass (m/z)	MS/MS	Error (ppm)	Molecular formula[a]	Annotation	FR3	FR4	Node	Ref.
29	12.40	177.0551[2]	177.0548[2]	163, 145, 135, 117, 89	−1.694	$C_{10}H_{10}O_4$	Ferulic acid[c]	x	–	5157	CCMSLIB00010111580
30	12.55	243.1021[2]	243.1017[2]	201, 189, 173, 159, 131	−1.645	$C_{15}H_{16}O_4$	Auraptenol[c] or CHEMBL3590439[sp], or Micromarin F[s]	–	x	1259	CCMSLIB00005722959
31	12.64	310.1654[3]	310.1650[3]	261, 243, 201, 189, 131	−1.290	$C_{16}H_{20}O_5$	❖Coumarin[c]	x	–	5130	CCMSLIB00004700679
32	12.65	389.1231	389.1233	374, 359, 356, 341, 328	0.514	$C_{20}H_{20}O_8$	5-Demethylnobiletin[b]	x	x	–	Kim et al., 2023
33	12.69	303.0868	303.0864	285, 177, 171, 163, 153	−1.320	$C_{16}H_{14}O_6$	Homoeriodictyol[c]	x	–	4951	CCMSLIB00003139732
34	12.71	303.0863	303.0865	285, 179, 177, 153	0.660	$C_{16}H_{14}O_6$	Hesperitin[b]	x	–	–	Kim et al., 2023
35	12.81	187.0395	187.0392	159, 143, 131, 115	−1.603	$C_{11}H_6O_3$	❖Furocoumarin[c]	x	–	4933	CCMSLIB00006423586
36	12.88	133.1017[2]	133.1014[2]	115, 105, 91	−2.254	$C_{10}H_{14}O$	Cumic Alcohol[c]	x	–	5086	CCMSLIB00005435949
37	13.02	201.1643[2]	201.1640[2]	173, 159, 145, 131, 119	−1.491	$C_{15}H_{22}O$	Nootkatone[c]	x	x	4184	CCMSLIB00010118710
38	10.66	345.0969	345.0969	345, 330, 315, 84	0.000	$C_{18}H_{16}O_7$	5,3′-Dihydroxy-3,7,4′-trimethoxyflavone[b]	–	–	–	Xu et al., 2018
39	13.66	217.0495	217.0497	202, 174, 161, 131, 115	0.921	$C_{12}H_8O_4$	Bergapten[b]	x	x	–	Yu et al., 2020
40	13.75	207.0652	207.0650	207, 192, 179, 151	−0.966	$C_{11}H_{10}O_4$	Scoparone[b]	x	–	–	Kim et al., 2023
41	13.82	419.1337	419.1339	419, 404, 389, 371	0.477	$C_{21}H_{22}O_9$	7-Hydroxy-3,5,6,8,3′,4′-hexamethoxyflavone[b]	x	x	–	Xu et al., 2018
42	13.93	359.1125	359.1126	359, 329, 311, 197	0.278	$C_{19}H_{18}O_7$	5-Hydroxy-6,7,8,4′-tetramethoxyflavone[b]	x	–	–	Xu et al., 2018
43	13.99	373.1287	373.1284	358, 343, 328, 312	−0.804	$C_{20}H_{20}O_7$	Sinensetin[c]	x	x	1165	CCMSLIB00010104830
44	14.14	343.1176	343.1177	328, 313, 285	0.291	$C_{19}H_{18}O_6$	4′,5,6,7-Tetramethoxyflavone[b]	–	–	–	Yu et al., 2020
45	14.29	135.1173[2]	135.1170[2]	107, 105, 93, 91, 79	−2.220	$C_{10}H_{16}O$	Carveol[c]	x	x	1947	CCMSLIB00010125872
46	14.46	231.1016	231.1018	175, 147, 119, 91	0.865	$C_{14}H_{14}O_3$	Osthenol[b]	x	x	–	Xu et al., 2018

(*continued on next page*)

Table 1 (*continued*)

Feature	R_t (min)	$[M+H]^+$; $^2[M+H\text{-}H_2O]^+$; $^3[M+NH_4]^+$; $^4[M+Na]^+$									
		Theoretical mass (*m/z*)	Measured mass (m/z)	MS/MS	Error (ppm)	Molecular formula[a]	Annotation	FR3	FR4	Node	Ref.
47	14.61	473.2170	473.2174	427, 279, 161	0.845	$C_{26}H_{32}O_8$	Deacetylnomilin[b]	–	–	–	Pessoa et al., 2021
48	14.71	403.1387	403.1391	388, 373, 355, 327, 301	0.992	$C_{21}H_{22}O_8$	Nobiletin[b]	x	x	–	Xu et al., 2018
49	15.22	433.1497	433.1493	403, 388, 385, 360, 165	−0.923	$C_{22}H_{24}O_9$	3′,4′,5′,3,5,6,7-Heptamethoxyflavone[b]	x	x		Wang et al., 2021
50	15.23	433.1498	433.1497	418, 403, 385, 373, 211	−0.231	$C_{22}H_{24}O_9$	3′,4′,5′,3,5,7,8-Heptamethoxyflavone[c]	x	x	1160	CCMSLIB00000847330
51	15.67	245.1177	245.1173	189, 161, 131, 103	−1.632	$C_{15}H_{16}O_3$	Osthole[c] or Suberosin[s]	x	–	4910	CCMSLIB00010107493
52	15.67	279.1232	279.1231	243, 189, 175, 149, 131	−0.358	$C_{15}H_8O_5$	Meranzin Hydrate[d] or Ulopterol[s]	–	x	1312	CCMSLIB00004696513
53	16.24	237.1126	237.1123	219, 191, 165, 149, 135	−1.265	$C_{13}H_{16}O_4$	❖Coumaran	x	x	1872	CCMSLIB00000851098
54	16.60	245.1177	245.1173	203, 189, 161, 131, 103	−1.632	$C_{15}H_{16}O_3$	Osthole[c] or Suberosin[s]	x	x	1168	CCMSLIB00010107493
55	17.04	243.1021[2]	243.1016[2]	201, 189, 173, 159, 131	−2.057	$C_{15}H_{16}O_4$	Auraptenol[c] or CHEMBL3590439[sp], or Micromarin F[s]	–	x	1175	CCMSLIB00005722959
56	17.10	315.1960	315.1956	269, 199, 187, 171, 131	−1.269	$C_{20}H_{26}O_3$	❖Diterpenoid[c]	x	x	1729	CCMSLIB00004699027
57	18.47	373.1282	373.1284	358, 343, 325, 312	0.536	$C_{20}H_{20}O_7$	Tangeritin[b]	x	x	–	Xu et al., 2018

[a] The molecular formulas described here refer to neutral monoisotopic masses. [b] Compound annotated only by manual dereplication. [c] Compound annotated only by the GNPS library. [d] Compound annotated by manual dereplication and the GNPS library. [s] Compound annotated by SIRIUS. [p] Pubchem code. ❖Chemical class (annotation level 3).

75, 76, 77, 78, 79 and 80).

In *O*-glycosylated flavonoids, there is the presence of a C—O bond connected to different sugars, which appears in the MS/MS spectra on electrospray ionization as characteristic neutral losses, such as 146 Da for a rhamnoside, *m/z* 162 for a glucoside and *m/z* 308 for a neohesperidoside losses (see **Supplementary Material**). The aglycone structure of flavonoids showed characteristic fragments (Fig. 4), such as $^{1,3}A^+$ (153 Da) and $^{1,3}B^+$, whose mechanism is *retro*-Diels-Alder type. It can be observed in flavones, flavanones, and flavonols. Other fragments present in the spectra were $^{0,2}A^+$, $^{0,2}B^+$, $^{0,3}B^+$, and $^{1,4}B^+$ formed from cleavages in the aglycone skeleton (Ma, Li, Van den Heuvel, & Claeys, 1997).

The *C*-glycosylated flavonoids joined by a C—C bond, such as compounds 18, 1N, and 2N (Table 1 and **Supplementary Table 3**), showed the base peak referring to the $^{0,2}X^+$ fragment at *m/z* 120. The presence of 90 Da fragments corresponding to the $^{0,3}X^+$ ion is also notable; these are fragments of part of the glycone, whose mechanism is cross-cleavage (Cuyckens & Claeys, 2004), as shown in Fig. 4.

All the flavonoids annotated by the GNPS library showed excellent spectral match, and two of them were annotated as gold annotation by the GNPS library (flavonoids 12 and 21). This classification brings greater robustness to the annotation since a gold annotation is understood to present a higher level of spectral quality within the database, as it matches experimental spectra with spectra of pure substances of synthetic or isolated origins with complete structural characterization. In addition to the annotations classified as gold, some compounds present in the fractions were identified as level 1 by comparison with analytical standards, such as naringin (6), hesperidin (16), and

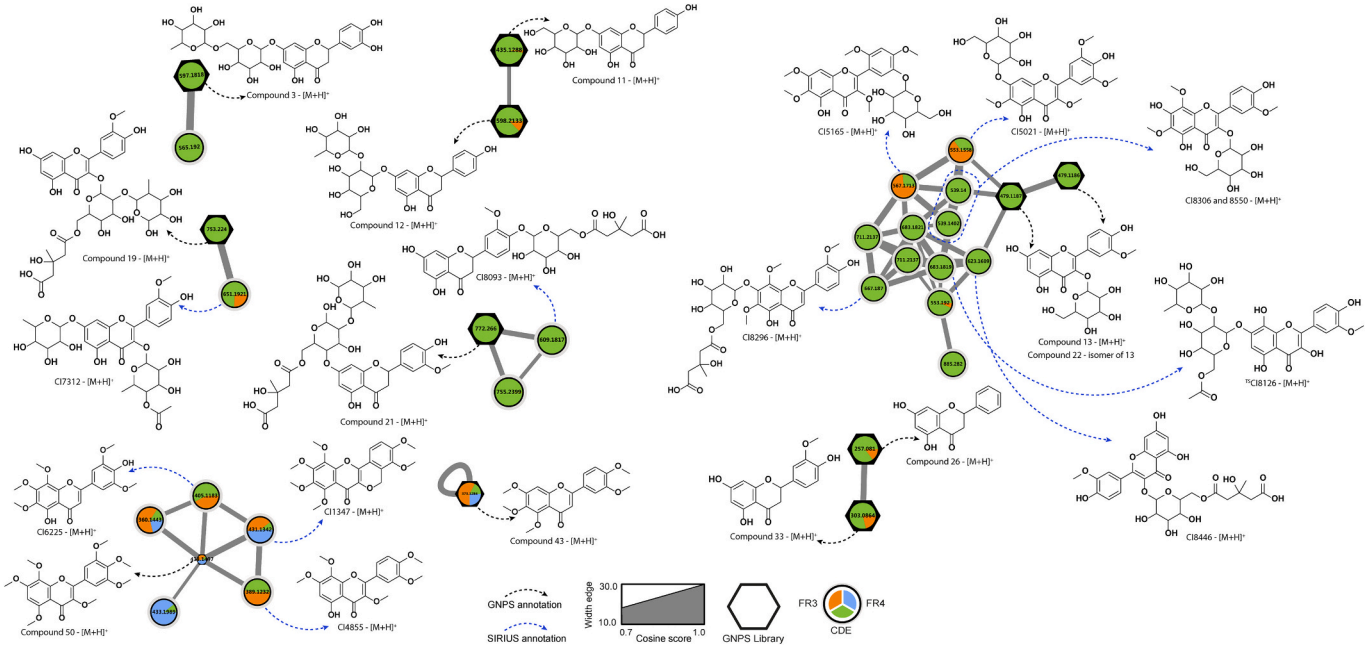

Fig. 3. Molecular families of flavonoids from the Feature-Based Molecular Networking workflow and annotation based on spectral matches in the public spectral libraries on the GNPS (black arrow) and SIRIUS (blue arrow). The pie chart legend shows that the different nodes' colors represent the sample groups (CDE, FR3, and FR4). Each node represents a mass spectrometry spectrum (MS/MS), and width edges represent MS/MS fragmentation similarity as a cosine score range between 0.7 (less thick) and 1.0 (thicker). The black diamond shape of some nodes represents the hits obtained by the GNPS spectral library, and the node size is proportional to a sum precursor intensity of features area in MS1 scans. The acronym CI (cluster index), followed by the values of the nodes found in the molecular network, refers to putative structural proposals based on the SIRIUS software. (For interpretation of the references to colour in this figure legend, the reader is referred to the web version of this article.)

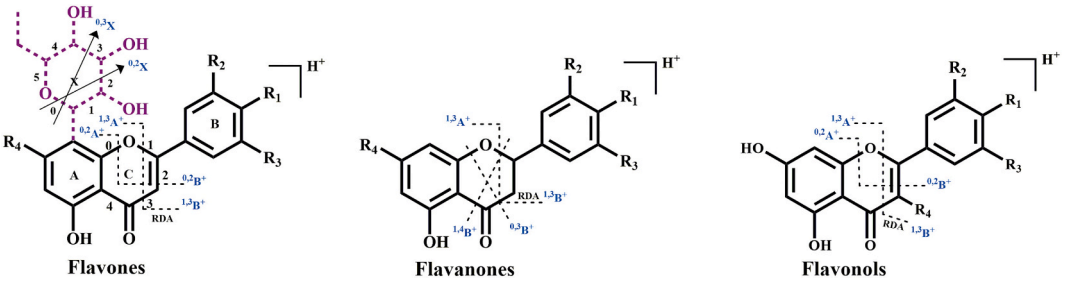

Fig. 4. Structure of flavonoid subclasses and the main fragmentations observed in MS/MS spectra.

hesperitin (34), founds in greater abundance in FR3 compared to FR4 (spectra are available in **Supplementary Fig. 10**, **Supplementary Fig. 26** and **Supplementary Fig. 48**).

The Fig. 3 also shows the presence of flavonoids containing a methoxyl and a sugar unit in the same structure, such as compounds 13 and 22, within the more prominent molecular family of flavonoids. Since these compounds have not yet been reported for the species, even though they are annotated by the GNPS spectral library, they were considered as level 3 annotations. From the annotation of these two compounds, it was possible to perform a structural propagation through the CSI:Finger ID module contained in SIRIUS. As a result, the putative structures of polymethoxylated flavonoids CI5165 and CI5020 were observed in nodes directly linked to compounds 13 and 22, which are present in greater abundance in fraction 3 when compared to CDE. This result reinforces that the compounds' presence in the fractions is due to their interaction with the mobile phase and stationary phase during SPE fractionation.

The partial absence of *O*-glycosylated flavonoids in fractions 3 and 4 (**Supplementary Fig. 106**) makes it possible to infer that they do not actively participate in the antifungal activity observed for these fractions and that other compounds, such as polymethoxyflavones, may be associated with the bioactivity, as will be discussed below. From this perspective, the presence of flavones belonging to the polymethoxyflavone subclass was also noted, and these were more abundant in the active fractions. As illustrated in Fig. 3, it is possible to observe a molecular family containing a node referring to compound 50 and three other polymethoxyflavones (CI4855, CI1347, and CI6225) employing structural propagation using the SIRIUS software. The spectral match obtained for compound 50 and the fragmentation trees for the structures obtained by structural propagation is in the supplementary material in **Supplementary Fig. 67** and **Supplementary Fig. 94**, **Supplementary Fig. 93**, and **Supplementary Fig. 92**.

The annotated polymethoxyflavones (32, 38, 41, 42, 43, 44, 48, 49, 50, and 57) showed a similar spectral pattern, with the most intense peaks corresponding to the protonated molecule $[M + H]^+$ and the loss of the $2CH_3$ fragments associated with the adduct $[M + H\text{-}(2CH_3)]^+$, at *m/z* 30. Between the two most abundant signals, this subclass showed a low-intensity peak equivalent to the loss of CH_3 (15 Da) expressed in the fragmentation spectra (Wang et al., 2021). (see **Supplementary Figs. 45**, **55**, **58**, **59**, **60**, **61**, **65**, **66**, **67**, and **74**).

The literature reports the antifungal activity of flavonoids of the flavanone subclass, such as eriodictiol (2), naringenin (9), and hesperitin (34), against fungi of the genus *Aspergillus*, *Candida*, and *Fusarium* (Aboody & Mickymaray, 2020). In consensus, Förster et al. (2022) investigated the activity of naringenin (9) and its *O*-methylated tautomers against two fungal species, *Fusarium graminearum*, and *Fusarium verticillioides*, and ultimately confirmed the antifungal potential of these phenolic compounds.

Among the 36 flavonoids that were annotated in this work, 10 of them are polymethoxyflavones (PMFs), which include tangeritin (57), nobiletin (48), 5-demethylnobiletin (32) and sinensetin (43). These compounds were previously found to be present in the peel of *Citrus reticulata Blanco* and showed inhibition against *Aspergillus niger*. The authors reported a minimum inhibitory concentration (MIC) of 1.5 mg/mL for tangeritin, a value close to that found for the alcoholic extract of *C. reticulata Blanco* bark. The explanation for the antifungal effects of polymethoxyflavones includes altering the permeability of the cytomembrane, causing fragility in the cell walls, and inhibiting chitin synthase, so they are considered natural antifungals that can be widely applied in the food industry (Wu et al., 2014).

Citrus species are known to have high levels of different classes of flavonoids in the composition of their peels, and several studies have reported that the fruit uses these compounds as a defense strategy against phytopathogenic fungi (Ortuño et al., 2011). Studies have shown that the fruit uses defense strategies through the accumulation of flavones (hesperidin, 16) and polymethoxyflavones (nobiletin, 48; heptametoxyflavone, 50, and tangeritin, 57) during infection by pathogenic fungi, such as *Penicillium digitatum* (Ortuño et al., 2006). This evidence reiterates that using these compounds, or products enriched with these compounds, can promote a fungicidal action against pathogens of different genera and species.

3.3.2. Coumarins

The two largest networks generated (Fig. 5A and B) showed library matches predominantly with coumarins. These compounds were also widely distributed in fractions 3 and 4 (orange and blue nodes) after fractionation, thus being associated with high values of mycelial inhibition presented for FR3 and FR4, as discussed above about fractionation efficiency applied.

The samples' coumarins belong to the lactonic compound class, derived from *O*-hydroxycinnamic acid and belonging to two subclasses: simple coumarins and furanocoumarins (Simões, 2007). Simple coumarins have a 1,2-benzopyrone nucleus containing hydroxyl, methoxyl, alkyl, and glycoside substituents. Among the 17 coumarins reported at level 2 in the present work, 13 are simple coumarins, with substances 5, 7, 23, 24, 25, 30, 31, 40, 46, 51, 52, 54, 55 presented in Table 1. Compounds 15, 31, and 35, which had yet to be reported for the *Citrus aurantium* species, were considered a level 3 annotation, with only the chemical class suggested in the annotation table.

On the other hand, furanocoumarins are characterized by containing a furan ring attached to the benzene ring (Simões, 2007; Bruni et al., 2019) and have been annotated as compounds 15, 27, 35, and 39 (Table 1 and **Supplementary Material**). In addition, a glycosylated furanocoumarin (compound 15) was found in the extract and bioactive fractions, whose base peak is formed by the loss of 162 Da, corresponding to one sugar unit.

In the MS/MS spectra of the simple coumarins and furanocoumarins present in the extract and the FR3 and FR4 fractions, it was possible to observe the loss of low molecular weight fragments, such as loss of H_2O, CH_3, and CO (Yu et al., 2020). In the MS/MS spectra of compounds 46, 51, and 54, the highest intensity signal was formed by the $[C_4H_8]^+$ fragment, whose *m/z* 56 corresponds to the loss of the alkyl group (prenyl) (Yu et al., 2020). Low abundance peaks were also observed in substances 27, 39, 40, and 46, corresponding to the formation of the tropylium cation $[C_7H_7]^+$ with an *m/z* 91, and the ion with an *m/z* 65, corresponding to the cyclopentadienylium cation $[C_5H_5]^+$ (Yu et al., 2020). The MS/MS spectra of all the substances listed can be found in the **Supplementary Material**.

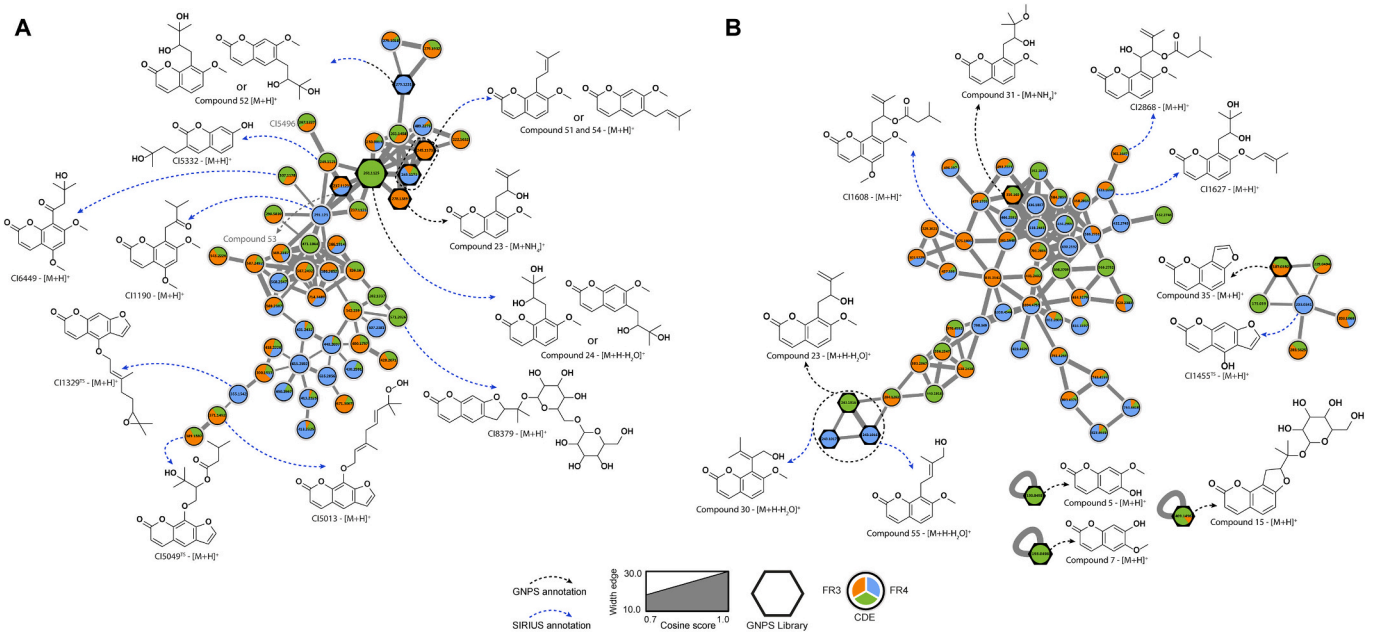

Fig. 5. (**A**) and (**B**) Molecular families with coumarins as major compounds obtained from the Feature-Based Molecular Networking workflow and annotated based on spectral matches in the GNPS (black arrow) and SIRIUS (blue arrow) public spectral libraries. The pie chart legend shows that the different nodes' colors represent the sample groups (CDE, FR3, and FR4). Each node represents a mass spectrometry spectrum (MS/MS), and width edges represent MS/MS fragmentation similarity as a cosine score range between 0.7 (less thick) and 1.0 (thicker). The black diamond shape of some nodes represents the hits obtained by the GNPS spectral library, and the node size is proportional to a sum precursor intensity of features area in MS1 scans. The acronym CI (cluster index), followed by the values of the nodes found in the molecular network, refers to structural proposals based on the SIRIUS software. (For interpretation of the references to colour in this figure legend, the reader is referred to the web version of this article.)

Among the annotations present in the molecular network A (Fig. 5), matches were obtained corresponding to compounds (24, 51, 52, and 54) that are structurally distinct only in the position of the substituent, but belong to the same chemical class, have the same exact mass and the same molecular formula. This limitation in annotation comes up against the similarity of these isomers in terms of MS/MS fragmentation, given that the GNPS spectral library is limited and dependent on the deposit of spectra by other users. This fact explains why most of the nodes that make up the networks were not annotated; however, even starting from a few spectral matches, it was possible to propagate the annotation and provide a greater knowledge of the structures putatively present in the active fractions.

As observed for the flavonoids, it was also possible to obtain annotations classified as gold for the furanocoumarins in the molecular network, such as compounds 5, 15, and 35. Specifically for compound 35, which clustered with other nodes in a smaller network, it was possible to perform structural propagation using the SIRIUS software. An adjacent node with predominant abundance in FR4 was proposed (1455^{TS}, see **Supplementary Table 5**) as bergaptol, a compound containing one less hydroxyl group and a change in the position of the furan ring in its structure when compared to compound 35, an analog of psoralen. All the fragmentation trees obtained for the structural propagation by the SIRIUS software are available in the supplementary material.

The achievement of structures proposed specified as "Training set" (TS), as obtained for compound 1455 and other compounds of the furanocoumarin class (1329 and 5049, see **Supplementary Table 5**), points above all to the excellent quality of the structure propagation based on the predictive model trained using a database of experimental and theoretical data used to build the internal library of the SIRIUS software. Consequently, it was also possible to infer that the experimental data obtained for the fractions from the LC-MS/MS analyses are of high quality, allowing for greater reliability of the compound annotation process presented here.

An example of a structural propagation based on the SIRIUS software is for compound 1329^{TS}, identified as an *O*-prenylated furanocoumarin called epoxybergamottin, derived from bergamottin since its only difference is the presence of an epoxide in the final double bond of the prenyl group. Furanocoumarins like this and others proposed here by SIRIUS as being present in the active fractions have already been shown to be components of various *Citrus* species, specifically in the fruit peels (Dugrand et al., 2013).

Coumarins are present in many *Citrus* species and are one of the most described classes of compounds with antimicrobial activity. Montagner et al. (2008) evaluated the antifungal activity of disubstituted structures such as scopoletin (7) and trisubstituted structures such as osthenol (46) and bergapten (39) against fungi of the genus *Fusarium*, *Candida* and *Aspergillus*. Trisubstituted coumarins have shown excellent antifungal results, especially in terms of prenylated coumarins such as osthenol (46). This activity is associated with an increase in the molecule's lipophilicity, which facilitates its permeation through the lipid layer.

As has been reported for flavonoids, several studies point to compounds from the coumarin class in the response to infection by phytopathogenic fungi. An example of this is the study carried out by Massana-Codina et al. (2020), in which it was possible to observe the pronounced accumulation of different coumarins during the infection of potatoes (*Solanum tuberosum*) by the pathogen *Colletotrichum coccodes*. Among the coumarins involved, scopoletin (7) showed antifungal activity against the potato pathogen, suggesting that the accumulation of coumarins is induced during infection by *C. coccodes* to limit the proliferation of the phytopathogen. This natural strategy used by different hosts allows us to potentially use the mechanisms existing in nature as promising control strategies for pests that affect significant commodities, such as yellow melon rot caused by *Fusarium jinanense*.

4. Conclusion

The application of current methodologies to explore and characterize different matrices to add value within the food industry allows us to discover and redirect the use of different unexploited residues. Among the various possibilities involving the production of waste from the citrus industry, this work enabled the chemical characterization of an essential oil residue from *Citrus aurantium* as well as proving its efficiency in inhibiting the fungus *Fusarium jinanense*, which causes yellow melon rot.

Using a robust and efficient workflow based on SPE fractionation, UHPLC-MS/MS analysis and the use of molecular networking associated with different databases and softwares (GNPS and SIRIUS), it was possible to annotate 65 metabolites from different chemical classes distributed within the crude extract and active fractions from the *C. aurantium* decoction. Compounds from the class of polymethoxyflavones, coumarins and furanocoumarins were mostly present in the fractions that were responsible for inhibiting 61% of the mycelial growth of the fungus *F. jinanense*, a value higher than that achieved by the current antifungal Cercobin® (48%) used in the field.

Our results show the potential of the essential oil composition residue and demonstrate the importance of understanding this residue at a molecular level so that it is possible to plan new studies aimed at developing new eco-friendly products and understanding the mechanisms of action of the compounds presented here against this harmful causal agent responsible for significant losses in melon production.

CRediT authorship contribution statement

Maria Daiane de Freitas: Writing – review & editing, Writing – original draft, Visualization, Validation, Resources, Project administration, Methodology, Investigation, Data curation, Conceptualization. **Rodolfo Dantas Lima Junior:** Writing – review & editing, Writing – original draft, Visualization, Validation, Software, Resources, Project administration, Methodology, Investigation, Formal analysis, Data curation, Conceptualization. **Francisco Erivaldo Freitas da Silva:** Methodology, Investigation, Data curation, Conceptualization. **Eliane Mayumi Inokuti:** Writing – review & editing, Writing – original draft, Methodology, Investigation, Data curation, Conceptualization. **Andréia Hansen Oster:** Writing – review & editing, Writing – original draft. **Davila Zampieri:** Writing – review & editing, Supervision. **Cristiano Souza Lima:** Writing – review & editing, Writing – original draft, Supervision, Methodology, Funding acquisition. **Taicia Pacheco Fill:** Writing – review & editing, Writing – original draft, Supervision, Project administration, Funding acquisition. **Telma Leda Gomes de Lemos:** Writing – review & editing, Writing – original draft, Supervision, Project administration, Funding acquisition.

Declaration of competing interest

The authors declare that they have no known competing financial interests or personal relationships that could have appeared to influence the work reported in this paper.

Data availability

Data will be made available on request.

Acknowledgments

This study was financed by the Coordenação de Aperfeiçoamento de Pessoal de Nível Superior - (CAPES) - Funding Code 001 and 88887.474570/2020–00. The authors gratefully acknowledge the financial support of Conselho Nacional de Desenvolvimento Científico e Tecnológico (CNPq), Project n° 303273.2019–4, 161466/2021–4 and Fundação de Amparo à Pesquisa do Estado de São Paulo (FAPESP),

Project n° 2022/02992–0.

Appendix A. Supplementary data

Supplementary data to this article can be found online at https://doi.org/10.1016/j.foodchem.2024.139769.

References

Abo Elgat, W. A. A., Kordy, A. M., Böhm, M., Černý, R., Abdel-Megeed, A., & Salem, M. Z. M. (2020). *Eucalyptus camaldulensis*, *citrus aurantium*, and *citrus sinensis* essential oils as antifungal activity against aspergillus flavus, aspergillus niger, aspergillus terreus, and fusarium culmorum. *Processes, 8*(8). https://doi.org/10.3390/pr8081003

Aboody, M. S. A., & Mickymaray, S. (2020). Anti-fungal efficacy and mechanisms of flavonoids. *Antibiotics, 9*(2). https://doi.org/10.3390/antibiotics9020045

Adusumilli, R., & Mallick, P. (2017). Data conversion with ProteoWizard msConvert. In L. Comai, J. Katz, & P. Mallick (Eds.), *Proteomics. Methods in molecular biology, 1550*. New York, NY: Humana Press. https://doi.org/10.1007/978-1-4939-6747-6_23.

Bruni, R., Barreca, D., Protti, M., Brighenti, V., Righetti, L., Anceschi, L., … Pellati, F. (2019). Botanical sources, chemistry, analysis, and biological activity of furanocoumarins of pharmaceutical interest. *Molecules, 24*(11). https://doi.org/10.3390/molecules24112163

Cuyckens, F., & Claeys, M. (2004). Mass spectrometry in the structural analysis of flavonoids. *In Journal of Mass Spectrometry, 39*(1). https://doi.org/10.1002/jms.585

Degirmenci, H., & Erkurt, H. (2020). Chemical profile and antioxidant potency of *Citrus aurantium* L. flower extracts with antibacterial effect against foodborne pathogens in rice pudding. *Lebensmittel-Wissenschaft & Technologie, 126*. https://doi.org/10.1016/j.lwt.2020.109273

Deterre, S. C., Rega, B., Delarue, J., Teillet, E., & Giampaoli, P. (2014). Classification of commercial bitter orange essential oils (*Citrus aurantium* L.), based on a combination of chemical and sensory analyses of specific odor markers. *Journal of Essential Oil Research, 26*(4). https://doi.org/10.1080/10412905.2014.917337

Dugrand, A., Olry, A., Duval, T., Hehn, A., Froelicher, Y., & Bourgaud, F. (2013). Coumarin and furanocoumarin quantitation in citrus peel via ultraperformance liquid chromatography coupled with mass spectrometry (UPLC-MS). *Journal of Agricultural and Food Chemistry, 61*(45). https://doi.org/10.1021/jf402763t

Dührkop, K., Fleischauer, M., Ludwig, M., Aksenov, A. A., Melnik, A. V., Meusel, M., … Böcker, S. (2019). SIRIUS 4: A rapid tool for turning tandem mass spectra into metabolite structure information. *Nature Methods, 16*(4). https://doi.org/10.1038/s41592-019-0344-8

FAO-Food and Agriculture Organization. (2020). Citrus fruit fresh and processed-Statistical bulletin 2020. https://www.fao.org/3/cb6492en/cb6492en.pdf. Available at: Accessed on: 08 April 2023.

Fiehn, O., Robertson, D., Griffin, J., vab der Werf, M., Nikolau, B., Morrison, N., … Sansone, S. A. (2007). The metabolomics standards initiative (MSI). *Metabolomics, 3*(3). https://doi.org/10.1007/s11306-007-0070-6

Förster, C., Handrick, V., Ding, Y., Nakamura, Y., Paetz, C., Schneider, B., … Köllner, T. G. (2022). Biosynthesis and antifungal activity of fungus-induced O-methylated flavonoids in maize. *Plant Physiology, 188*(1). https://doi.org/10.1093/plphys/kiab496

Han, S. L., Wang, M. M., Ma, Z. Y., Raza, M., Zhao, P., Liang, J. M., … Cai, L. (2023). *Fusarium* diversity associated with diseased cereals in China, with an updated phylogenomic assessment of the genus. *Studies in Mycology, 104*. https://doi.org/10.3114/sim.2022.104.02

Horai, H., Arita, M., Kanaya, S., Nihei, Y., Ikeda, T., Suwa, K., … Nishioka, T. (2010). MassBank: A public repository for sharing mass spectral data for life sciences. *Journal of Mass Spectrometry, 45*(7). https://doi.org/10.1002/jms.1777

IBGE-Brazilian Institute of Geography and Statistics. (2023). Municipal Agricultural Production. https://sidra.ibge.gov.br/tabela/1612. Available at: Accessed on April 22, 2023.

Kim, S., Chen, J., Cheng, T., Gindulyte, A., He, J., He, S., … Bolton, E. E. (2023). PubChem 2023 update. *Nucleic Acids Research, 51*(D1). https://doi.org/10.1093/nar/gkac956

Kist, B. B., Carvalho, D. C., & Beling, R. R. (2022). *Anuário Brasileiro de Horti&Fruti 2022 – Santa Cruz do Sul: Editora Gazeta Santa Cruz* (pp. 62–65). https://www.editoragazeta.com.br/sitewp/wp-content/uploads/2022/04/HORTIFRUTI_2022.pdf. Available at: Accessed on April 14, 2023.

Lima, E. N., Oster, A. H., Bordallo, P. N., Araújo, A. A. C., Silva, D. E. M., & Lima, C. S. (2021). A novel lineage in the fusarium incarnatum-equiseti species complex is one of the causal agents of fusarium rot on melon fruits in Northeast Brazil. *Plant Pathology, 70*(1). https://doi.org/10.1111/ppa.13271

Ma, Y. L., Li, Q. M., Van den Heuvel, H., & Claeys, M. (1997). Characterization of flavone and flavonol aglycones by collision-induced dissociation tandem mass spectrometry. *Rapid Communications in Mass Spectrometry, 11*(12). https://doi.org/10.1002/(SICI)1097-0231(199708)11:12<1357::AID-RCM983>3.0.CO;2-9

Massana-Codina, J., Schnee, S., Allard, P. M., Rutz, A., Boccard, J., Michellod, E., … Wolfender, J. L. (2020). Insights on the structural and metabolic resistance of potato (*Solanum tuberosum*) cultivars to tuber black dot (Colletotrichum coccodes). *Frontiers in Plant Science, 11*. https://doi.org/10.3389/fpls.2020.01287

Medeiros Araújo, M. B., Moreira, G. M., Nascimento, L. V., Nogueira, G.d. A., Nascimento, S. R.d. C., Pfenning, L. H., & Ambrósio, M. M.d. Q. (2021). Fusarium rot of melon is caused by several Fusarium species. *Plant Pathology, 70*(3). https://doi.org/10.1111/ppa.13328

Mencherini, T., Campone, L., Piccinelli, A. L., García Mesa, M., Sánchez, D. M., Aquino, R. P., & Rastrelli, L. (2013). HPLC-PDA-MS and NMR characterization of a hydroalcoholic extract of *Citrus aurantium* L. var. amara peel with antiedematogenic activity. *Journal of Agricultural and Food Chemistry, 61*(8). https://doi.org/10.1021/jf302815t

Montagner, C., De Souza, S. M., Groposo, C., Delle Monache, F., Smânia, E. F. A., & Smânia, A. (2008). Antifungal activity of coumarins. *Zeitschrift fur Naturforschung C: Journal of Biosciences, 63*(1–2). https://doi.org/10.1515/znc-2008-1-205

Nair, H., & Clarke, W. (2016). Mass spectrometry for the clinical laboratory. *In Mass Spectrometry for the Clinical Laboratory.*. https://doi.org/10.1016/c2013-0-19099-x

Nothias, L. F., Petras, D., Schmid, R., Dührkop, K., Rainer, J., Sarvepalli, A., … Dorrestein, P. C. (2020). Feature-based molecular networking in the GNPS analysis environment. *Nature Methods, 17*(9). https://doi.org/10.1038/s41592-020-0933-6

Okwu, D. E., Awurum, A. N., & Okoronkwo, J. I. (2007). Phytochemical composition and in vitro antifungal activity screening of extracts from citrus plants against fusarium oxysporum of okra plant (*Hibiscus esculentus*). *Summa Phytopathologica, 30*, 145–148. https://api.semanticscholar.org/CorpusID:55533842.

Onakpoya, I., Davies, L., & Ernst, E. (2011). Efficacy of herbal supplements containing *Citrus aurantium* and synephrine alkaloids for the management of overweight and obesity: A systematic review. *Focus on Alternative and Complementary Therapies, 16*(4). https://doi.org/10.1111/j.2042-7166.2011.01115.x

Ortuño, A., Báidez, A., Gómez, P., Arcas, M. C., Porras, I., García-Lidón, A., & Del Río, J. A. (2006). Citrus paradisi and *Citrus sinensis* flavonoids: Their influence in the defence mechanism against Penicillium digitatum. *Food Chemistry, 98*(2). https://doi.org/10.1016/j.foodchem.2005.06.017

Ortuño, A., Díaz, L., Alvarez, N., Porras, I., García-Lidón, A., & Del Río, J. A. (2011). Comparative study of flavonoid and scoparone accumulation in different Citrus species and their susceptibility to Penicillium digitatum. *Food Chemistry, 125*(1). https://doi.org/10.1016/j.foodchem.2010.09.012

Oulebsir, C., Mefti-Korteby, H., Djazouli, Z. E., Zebib, B., & Merah, O. (2022). Essential oil of *Citrus aurantium* L. leaves: Composition, antioxidant activity, elastase and collagenase inhibition. *Agronomy, 12*(6). https://doi.org/10.3390/agronomy12061466

Perczak, A., Gwiazdowska, D., Marchwińska, K., Juś, K., Gwiazdowski, R., & Waśkiewicz, A. (2019). Antifungal activity of selected essential oils against *Fusarium culmorum* and F. graminearum and their secondary metabolites in wheat seeds. *Archives of Microbiology, 201*(8). https://doi.org/10.1007/s00203-019-01673-5

Pessoa, L. G. A., Pessoa, L. A., Santos, É.d. S., Pilau, E. J., Gonçalves, J. E., Gonçalves, R. A. C., & de Oliveira, A. J. B. (2021). Limonoid detection and profile in callus culture of sweet orange. *Acta Scientiarum-Biological Science, 43*. https://doi.org/10.4025/actascibiolsci.v43i1.53075

Pluskal, T., Castillo, S., Villar-Briones, A., & Oresic, M. (2010). MZmine 2: Modular framework for processing, visualizing, and analyzing mass spectrometry-based molecular profile data. *BMC Bioinformatics, 11*. https://doi.org/10.1186/1471-2105-11-395

Schymanski, E. L., Jeon, J., Gulde, R., Fenner, K., Ruff, M., Singer, H. P., & Hollender, J. (2014). Identifying small molecules via high resolution mass spectrometry: Communicating confidence. *In Environmental Science & Technology, 48*. https://doi.org/10.1021/es5002105

Shannon, P., Markiel, A., Ozier, O., Baliga, N. S., Wang, J. T., Ramage, D., … Ideker, T. (2003). Cytoscape: A software environment for integrated models of biomolecular interaction networks. *Genome Research, 13*. https://doi.org/10.1101/GR.1239303

Simionato, A. S., Navarro, M. O. P., de Jesus, M. L. A., Barazetti, A. R., da Silva, C. S., Simões, G. C., … de Oliveira, A. G. (2017). The effect of phenazine-1-carboxylic acid on mycelial growth of *Botrytis cinerea* produced by *Pseudomonas aeruginosa* LV strain. *Frontiers in Microbiology, 8*. https://doi.org/10.3389/fmicb.2017.01102

Simões, C. M. O. (2007). Farmacognosia: da planta ao medicamento 6. In *Porto Alegre: Editora da UFRGS; Florianópolis: Editora da UFSC* (pp. 537–555).

Sumner, L. W., Amberg, A., Barrett, D., Beale, M. H., Beger, R., Daykin, C. A., … Viant, M. R. (2007). Proposed minimum reporting standards for chemical analysis. *Metabolomics, 3*(3). https://doi.org/10.1007/s11306-007-0082-2

Wang, Q., Zou, Z., Zhang, Y., Lin, P., Lan, T., Qin, Z., Xu, D., Wu, H., & Yao, Z. (2021). Characterization of chemical profile and quantification of major representative components of Wendan decoction, a classical traditional Chinese medicine formula. *Journal of Separation Science, 44*(5). https://doi.org/10.1002/jssc.202000952

Wen, L., He, M., Yin, C., Jiang, Y., Luo, D., & Yang, B. (2021). Phenolics in *Citrus aurantium* fruit identified by UHPLC-MS/MS and their bioactivities. *Lebensmittel-Wissenschaft & Technologie, 147*. https://doi.org/10.1016/j.lwt.2021.111671

Wu, T., Cheng, D., He, M., Pan, S., Yao, X., & Xu, X. (2014). Antifungal action and inhibitory mechanism of polymethoxylated flavones from *Citrus reticulata* Blanco peel against Aspergillus niger. *Food Control, 35*(1). https://doi.org/10.1016/j.foodcont.2013.07.027

Xu, Y., Cai, H., Cao, G., Duan, Y., Pei, K., Tu, S., … Shen, L. (2018). Profiling and analysis of multiple constituents in Baizhu Shaoyao san before and after processing by stir-frying using UHPLC/Q-TOF-MS/MS coupled with multivariate statistical analysis. *Journal of Chromatography B: Analytical Technologies in the Biomedical and Life Sciences, 1083*. https://doi.org/10.1016/j.jchromb.2018.03.003

Yu, L., Chen, M., Liu, J., Huang, X., He, W., Qing, Z., & Zeng, J. (2020). Systematic detection and identification of bioactive ingredients from *Citrus aurantium* L. var. amara using HPLC-Q-TOF-MS combined with a screening method. *Molecules, 25*(2). https://doi.org/10.3390/molecules25020357

Zakaria, L. (2023). Fusarium species associated with diseases of major tropical fruit crops. *Horticulturae, 9*(3). https://doi.org/10.3390/horticulturae9030322